Available online at www.sciencedirect.com
ScienceDirect
Atmospheric Environment 42 (2008) 1476–1490
ATMOSPHERIC ENVIRONMENT
www.elsevier.com/locate/atmosenv

Oligomers formed through in-cloud methylglyoxal reactions: Chemical composition, properties, and mechanisms investigated by ultra-high resolution FT-ICR mass spectrometry

K.E. Altieri[a,*], S.P. Seitzinger[a,b], A.G. Carlton[c], B.J. Turpin[d], G.C. Klein[e], A.G. Marshall[f,g]

[a]*Institute of Marine and Coastal Sciences, Rutgers University, 71 Dudley Road, New Brunswick, NJ 08901, USA*
[b]*Rutgers/NOAA CMER Program, Rutgers University, 71 Dudley Road, New Brunswick, NJ 08901, USA*
[c]*ASMD, ARL, NOAA, Mail Drop E-243-01, Research Triangle Park, NC 27711, USA*
[d]*Department of Environmental Sciences, Rutgers University, 14 College Farm Road, New Brunswick, NJ 08901, USA*
[e]*Department of Biology, Chemistry and Environmental Science, Christopher Newport University, 1 University Place, Newport News, VA 23606, USA*
[f]*Ion Cyclotron Resonance Program, National High Magnetic Field Laboratory, Florida State University, 1800 East Paul Dirac Drive, Tallahassee, FL 32310, USA*
[g]*Department of Chemistry and Biochemistry, Florida State University, Tallahassee, FL 32306, USA*

Received 24 August 2007; received in revised form 1 November 2007; accepted 1 November 2007

Abstract

Secondary organic aerosol (SOA) is a substantial component of total atmospheric organic particulate matter, but little is known about the composition of SOA formed through cloud processing. We conducted aqueous phase photo-oxidation experiments of methylglyoxal and hydroxyl radical to simulate cloud processing. In addition to predicted organic acid monomers, oligomer formation from methylglyoxal–hydroxyl radical reactions was detected by electrospray ionization mass spectrometry (ESI-MS). The chemical composition of the oligomers and the mechanism of their formation were investigated by ultra-high resolution Fourier transform ion cyclotron resonance mass spectrometry (FT-ICR MS) and LCQ DUO ion trap mass spectrometry (ESI-MS-MS). Reaction products included 415 compounds detected in the mass range 245–800 Da and the elemental composition of all 415 compounds were determined by ultra-high resolution FT-ICR MS. The ratio of total organic molecular weight per organic carbon weight (OM:OC) of the oligomers (1.0–2.5) was lower than the OM:OC of the organic acid monomers (2.3–3.8) formed, suggesting that the oligomers are less hygroscopic than the organic acid monomers formed from methylglyoxal–hydroxyl radical reaction. The OM:OC of the oligomers (average = 2.0) is consistent with that of aged atmospheric aerosols and atmospheric humic-like substances (HULIS). A mechanism is proposed in which the organic acid monomers formed through hydroxyl radical reactions oligomerize through esterification. The mechanism is supported by the existence of series of oligomers identified by elemental composition from FT-ICR MS and ion fragmentation patterns from ESI-MS-MS. Each oligomer series starts with an organic acid monomer formed from hydroxyl radical oxidation, and increases in molecular weight and total oxygen content through esterification with a hydroxy acid ($C_3H_6O_3$) resulting in multiple additions of 72.02113 Da ($C_3H_4O_2$) to the parent organic acid monomer. Methylglyoxal is a water-soluble product of both gas phase biogenic (i.e., isoprene) and anthropogenic (i.e., aromatics, alkenes) hydrocarbon oxidation. The varied and multiple sources of methylglyoxal increase

*Corresponding author. Tel.: +1 732 932 6555x368; fax: +1 732 932 1792.
E-mail address: altieri@marine.rutgers.edu (K.E. Altieri).

1352-2310/$ - see front matter
doi:10.1016/j.atmosenv.2007.11.015

the potential for these low volatility cloud processing products (e.g., oxalic acid and oligomers) to significantly contribute to SOA. Aqueous phase oligomer formation investigated here and aerosol phase oligomer formation appear to be more similar than previously realized, which may simplify the incorporation of oligomers into atmospheric SOA models.

Keywords: Methylglyoxal; Oligomers; Cloud processing; FT-ICR MS; SOA; Isoprene

1. Introduction

Atmospheric aerosols scatter and absorb light, influencing the global radiation budget and climate (IPCC, 2001), and are associated with adverse effects on human health (EPA, 2004). Secondary organic aerosol (SOA), a fraction of total organic aerosol, is formed through gas-to-particle conversion processes involving products of reactive organic gases (Jang et al., 2002; Seinfeld and Pankow, 2003). SOA formation through condensation/sorption of gas phase reaction products and subsequent aerosol phase reactions has been studied extensively and SOA constituents include oligomers and humic-like substances (HULIS) (Gao et al., 2004; Graber and Rudich, 2006; Kalberer et al., 2004; Reinhardt et al., 2007; Surratt et al., 2006; Tolocka et al., 2004). Ultra-high resolution Fourier transform ion cyclotron resonance mass spectrometry (FT-ICR MS) has been used to investigate SOA oligomers formed through smog chamber experiments (Kalberer et al., 2004; Reinhardt et al., 2007; Tolocka et al., 2004), and to analyze ambient aerosols (Denkenberger et al., 2007; Reemtsma et al., 2006). There is growing evidence that just as sulfate is formed through aqueous phase reactions, SOA is also formed through aqueous phase reactions in clouds, fogs and aerosols (Altieri et al., 2006; Blando and Turpin, 2000; Carlton et al., 2006, 2007; Ervens et al., 2003, 2004; Gelencser and Varga, 2005; Heald et al., 2006; Lim et al., 2005; Sorooshian et al., 2007).

Methylglyoxal is found widely in urban, rural, and remote environments (Kawamura et al., 1996; Kawamura and Yasui, 2005). Methylglyoxal is a secondary product formed from the oxidation and ozonolysis of anthropogenic hydrocarbons (e.g., aromatics, toluene, xylene) making it a potentially important contributor to SOA on urban and regional scales (Atkinson and Arey, 2003; Ham et al., 2006; Smith et al., 1999). It is also a secondary product from the oxidation of biogenic hydrocarbons (e.g., isoprene) (Atkinson, 2000; Atkinson and Arey, 2003). Because isoprene has a large world-wide emission flux, even small SOA yields from isoprene would have significant climate implications (Henze and Seinfeld, 2006). Recent smog chamber and aqueous photochemistry experiments suggest that isoprene is an SOA precursor (Altieri et al., 2006; Carlton et al., 2006, 2007; Kroll et al., 2006; Surratt et al., 2006).

There is experimental evidence that oligomeric products form through cloud processing: aqueous phase self-polymerization of methylglyoxal (Hastings et al., 2005; Loeffler et al., 2006), photo-induced self-oligomerization of aqueous pyruvic acid (Guzman et al., 2006), acid catalyzed aqueous phase reactions of levoglucosan (Holmes and Petrucci, 2006), and aqueous reaction of hydroxyl radical and pyruvic acid (Altieri et al., 2006; Carlton et al., 2006). The properties of oligomers formed through atmospheric aqueous phase photochemistry, the reaction mechanisms leading to oligomer formation and the resulting atmospheric implications for SOA produced through cloud processing, however, have not been elucidated.

The mechanism of oligomer formation and the properties of the oligomers formed through aqueous-phase photo-oxidation of methylglyoxal were investigated in this study. Oligomers were detected by ESI-MS analysis of time series samples. Their chemical composition and formation mechanism were investigated by ultra-high resolution FT-ICR MS (Marshall et al., 1998). Evidence for the proposed structures of the oligomers and the proposed mechanism of formation was provided by ESI-MS-MS. Implications for SOA produced through cloud processing are discussed. To our knowledge this is the first description of the chemical composition and formation mechanism of oligomers formed through aqueous phase reactions relevant to atmospheric waters.

2. Experimental

Batch photochemical aqueous phase reactions of methylglyoxal (2 mM) and hydrogen peroxide (10 mM) were conducted in triplicate in 1 L

borosilicate vessels under conditions encountered by cloud water (pH 4.2–4.5). The concentrations in the experiment are higher than those in cloud and fog droplets (Matsumoto et al., 2005), but lower than those in aerosol water (Munger et al., 1995). The UV irradiation of hydrogen peroxide was the source of hydroxyl radicals in the reaction vessel. The UV source was a low-pressure monochromatic (254 nm) mercury lamp placed in a quartz immersion well. The details of the experimental setup are described elsewhere (Altieri et al., 2006; Carlton et al., 2006, 2007). Briefly, a $t = 0$ min sample was taken from the volumetric flask used to prepare the solution, and then samples were taken from the reaction vessel every 20–30 min for the duration of the experiment (~6.5 h). A 0.5% aqueous catalase solution was used to destroy the hydrogen peroxide (0.25 μL/1 mL sample) (Stefan et al., 1996). The samples were stored in the dark in the freezer until analysis. For each experiment there were two control experiments: (1) UV control (methylglyoxal plus UV with no H_2O_2 added) and (2) H_2O_2 control (methylglyoxal plus H_2O_2 with no UV).

2.1. ESI-MS

All experimental samples discussed below were analyzed with an HP-Agilent 1100 atmospheric pressure electrospray ionization mass spectrometer with a quadrupole mass-selective detector. A liquid chromatograph (LC) autosampler was used to inject sample solutions (six replicate injections, 20 μL each) from individual vials into the LC system; no column was used in these analyses. The mobile phase was 60:40 (v/v) 100% methanol and 0.05% formic acid in deionized water with a flow rate of 0.220 mL min^{-1}. Experimental samples, controls, and standards were analyzed as negative and positive ions (mass range 50–1000 Da, fragmentor voltage 40 V, capillary voltage 3 kV). The ion abundance of any m/z detected in the deionized water blank was subtracted from the spectra of all experimental samples, controls, and standards. Nitrogen was the drying gas (350 °C, 24 psig, 10 L min^{-1}). The unit mass resolution spectra were recorded with Agilent software (Chemstation version A.07.01) and exported to Access and Excel (Microsoft, Inc.) for statistical analysis and interpretation as described previously (Altieri et al., 2006). A mixed standard of methylglyoxal, pyruvic acid, acetic acid, glyoxylic acid, and oxalic acid (precursor and expected monomeric products) in the same matrix as samples (H_2O_2 1:5 ratio, 1 μL catalase) was analyzed under the same instrument conditions as experimental time series samples. Methylglyoxal was detected as a proton-bound positive-ion dimer $(2M+H)^+$. Pyruvic, glyoxylic, and oxalic acids were detected as negative ions $(M-H)^-$. Acetic acid is not detected by ESI-MS as discussed previously (Altieri et al., 2006), but its presence was verified by HPLC (Carlton, 2006).

2.2. Ultra-high resolution electrospray ionization FT-ICR MS

Analyses were performed on a 69 min experimental time series sample with a 9.4-T Fourier transform ion cyclotron resonance mass spectrometer equipped with an ESI source at the National High Magnetic Field Laboratory (NHMFL) (Marshall and Guan, 1996; Senko et al., 1996, 1997). The needle voltage was ±2000 V, the heated capillary current was ~3.5 A, and the tube lens was ±350 V. Ions were accumulated external to the magnet in a linear octopole ion trap (25.1-cm-long) equipped with axial electric field (Wilcox et al., 2002) and transferred through rf-only multipoles to a 10-cm-diameter, 30-cm-long open cylindrical Penning ion trap. Multipoles were operated at: 1.6 MHz/0.5 V_{p-p}, 1.7 MHz/0.5 V_{p-p}, 1.8 MHz/1.4 V_{p-p}. The data were zero-filled, Hamming apodized, and then processed by Fourier transform and magnitude computation. The spectra were mass calibrated with standard ions with an internal calibrant (G2421A Agilent "tuning mix") and MIDAS Analyzer software. The residual root-mean-square mass error after internal calibration was 0.42 ppm.

MIDAS Formula Calculator Software (v1.1) was used to calculate all mathematically possible formulas for all ions detected with a mass tolerance of ±1 ppm. An unlimited number of ^{12}C, ^{1}H, ^{16}O and one ^{13}C were allowed in the molecular formula calculations. There were 446 ions where only one chemical formula containing ^{12}C, ^{1}H, and ^{16}O was possible, within ±1 ppm of the measured mass. Elemental formulas with a ^{13}C were checked for the ^{12}C counterpart; if it was not present the ^{13}C formula was deleted. This process eliminated 31 formulas, including all four compounds that had multiple assigned molecular formulas. The average mass error for all assignments was 0.67 ppm for the 446 ions identified. Ions were also characterized by the number of rings plus double bonds (i.e., double bond equivalents (DBE)), calculated from Eq. (1)

(McLafferty and Turecek, 1993):

$$\mathrm{DBE} = c - \tfrac{1}{2}h + 1 \quad \text{for elemental composition, } C_cH_hO_o \tag{1}$$

2.3. Comparison of ESI-MS and FT-ICR MS spectra

The ESI-MS was used to analyze a mass range of 50–1000 Da and the FT-ICR MS was used to analyze a mass range of 245–1200 Da. The overlap range of $300 < m/z < 500$ was arbitrarily chosen and used to compare the output from the two mass spectrometers for the same sample ($t = 69$ min). There is excellent agreement in the masses detected when the sample is analyzed by both ESI-MS and FT-ICR MS (Fig. S-1). At unit mass resolution, 45% of the ions detected have two compounds in the unit mass bin detected by FT-ICR MS, and 13% of the ions detected have more than two compounds present in the unit mass bin. The relative ion abundance pattern is also conserved for the masses in the overlapping section in both mass spectrometers.

2.4. ESI-MS-MS

The Finnigan LCQ Duo quadrupole ion trap mass spectrometer (San Jose, CA) (ESI-MS-MS) was used to obtain further structural information for ions of a select number of masses. The samples were infused directly into the mass spectrometer at 0.033 mL min^{-1}. The spray voltage was −4 kV with a capillary temperature of 150 °C. The capillary voltage was −13 V with the sheath gas flow rate (arbitrary units) set at 96 and the auxiliary gas flow rate at 5. The ion optics were set as follows: octopole 1 offset 6.5 V, octopole 2 offset 9 V, inter-octopole lens 32 V, and the tube lens 10 V. Collision-induced dissociation (CID) negative ion spectra were obtained with normalized collision energies of 20–30%.

3. Results and discussion

3.1. Organic acid monomer formation

The appearance of organic acids in the ESI mass spectrum is consistent with the methylglyoxal photo-oxidation mechanism used by Lim et al. (2005) and the results of pyruvic acid photo-oxidation experiments (Altieri et al., 2006; Carlton et al., 2006) (Fig. 1, solid arrows). The precursor methylglyoxal reacts almost immediately with little remaining in the first time series sample ($t = 0$ min; positive ion data not shown). Pyruvic acid (m/z 87) and glyoxylic acid (m/z 73), two of the originally hypothesized intermediates to oxalic acid formation, are low in ion abundance (<1000 abundance units) throughout the experiment. Oxalic acid (m/z 89) forms over time and is the dominant peak in the last time series sample (Fig. 2). This result is similar to previous pyruvic acid photo-oxidation experiments wherein the pyruvic acid reacted quickly, the glyoxylic acid ion abundance remained low throughout the experiment, and oxalic acid was an end product (Altieri et al., 2006; Carlton et al., 2006).

3.2. Oligomer formation

In addition to the organic acid monomers, after ~35 min of photo-oxidation we observe a large number of compounds (Fig. 2) that are of a higher molecular weight than the precursor and products in the reaction scheme used by Lim et al. (2005) (Fig. 1). The complexity of the ESI-MS spectra increases with time (until $t = 69$ min) and there is a regular pattern of mass differences (12, 14, 16 Da) in the higher molecular weight products (Figs. 2 and 3) indicating an oligomer system (Kalberer et al., 2004; Reinhardt et al., 2007; Tolocka et al., 2004). The oligomer system develops over time, reaching maximum ion abundances for most peaks at ~69 min and then decreasing in ion abundance as other products form (e.g., m/z 89 oxalic acid, m/z 103, 133, 177). The complexity of the experimental time series spectra and the simplicity of the mixed standard spectra (Fig. 4) reaffirm that oligomer formation is not an artifact of the ESI process. The oligomers and oxalic acid/oxalate (Martinelango et al., 2007) are both low volatility products that will contribute to SOA upon cloud droplet evaporation.

The oligomer pattern in the aqueous methylglyoxal–hydroxyl radical reaction time series sample spectra is almost identical to that for oligomers seen in aqueous pyruvic acid–hydroxyl radical experiments previously described (Altieri et al., 2006). At maximal oligomer formation, the methylglyoxal experimental sample exhibited 296 ions whereas the pyruvic acid experimental sample showed 249 ions, with 230 ions present in both spectra (mass range 50–500 Da, ESI-MS). This result is consis-

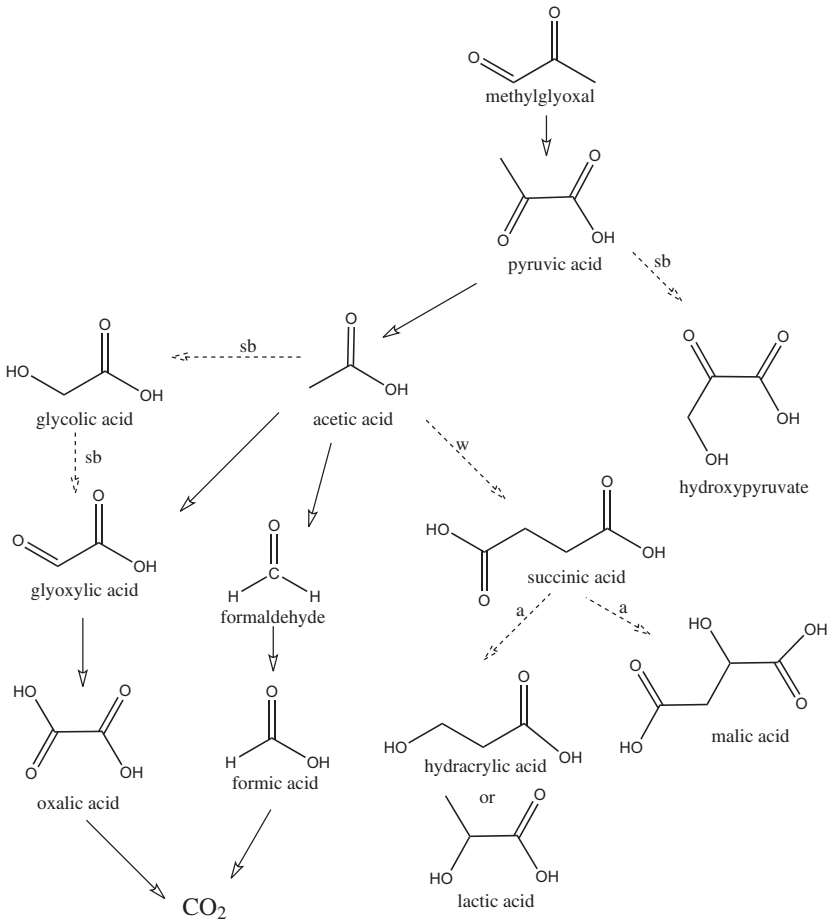

Fig. 1. Proposed mechanism of aqueous phase photo-oxidation of methylglyoxal and hydroxyl radical leading to organic acid monomers that then participate in oligomerization reactions. The dotted line labeled "a" is original to this work. The solid arrows represent the mechanism used by Lim et al. (2005) originally from Stefan et al. (1996) and Stefan and Bolton (1999) whereas the dashed lines labeled "sb" indicate reactions taken from Stefan et al. (1996) and Stefan and Bolton (1999) that were not outlined in Lim et al. (2005). The dashed line labeled "w" is a reaction taken from Wang et al. (2001). All reactions proceed via the hydroxyl radical.

tent with the mechanism used by Lim et al. (2005) (Fig. 1) in which pyruvic acid is produced from aqueous methylglyoxal oxidation. Initiating reactions with methylglyoxal rather than pyruvic acid caused almost no change in the oligomer distribution, indicating that oligomer formation does not require the presence of methylglyoxal, only its reaction products (e.g., pyruvic acid, acetic acid, formic acid). Although hydration of aldehydes and subsequent self-polymerization have been hypothesized as an aqueous phase SOA formation pathway (Hastings et al., 2005), we found no evidence that this mechanism contributes to oligomer formation from methylglyoxal when hydroxyl radicals are present, either because the concentrations used in these experiments are too low for self-polymerization, or the oligomer formation mechanism that occurs when hydroxyl radical is present is the dominant oligomer formation mechanism.

3.2.1. Control samples

In the UV control experiment (methylglyoxal plus UV, no H_2O_2) and the H_2O_2 control experiment (methylglyoxal plus H_2O_2, no UV), no significant product formation was observed by ESI-MS (Fig. S-2) indicating that the oligomer formation is due to the reaction of methylglyoxal with the hydroxyl radical, and not hydrogen peroxide or UV light alone. This is consistent with previously reported in-cloud oligomer formation through pyruvic acid photo-oxidation (Altieri et al., 2006).

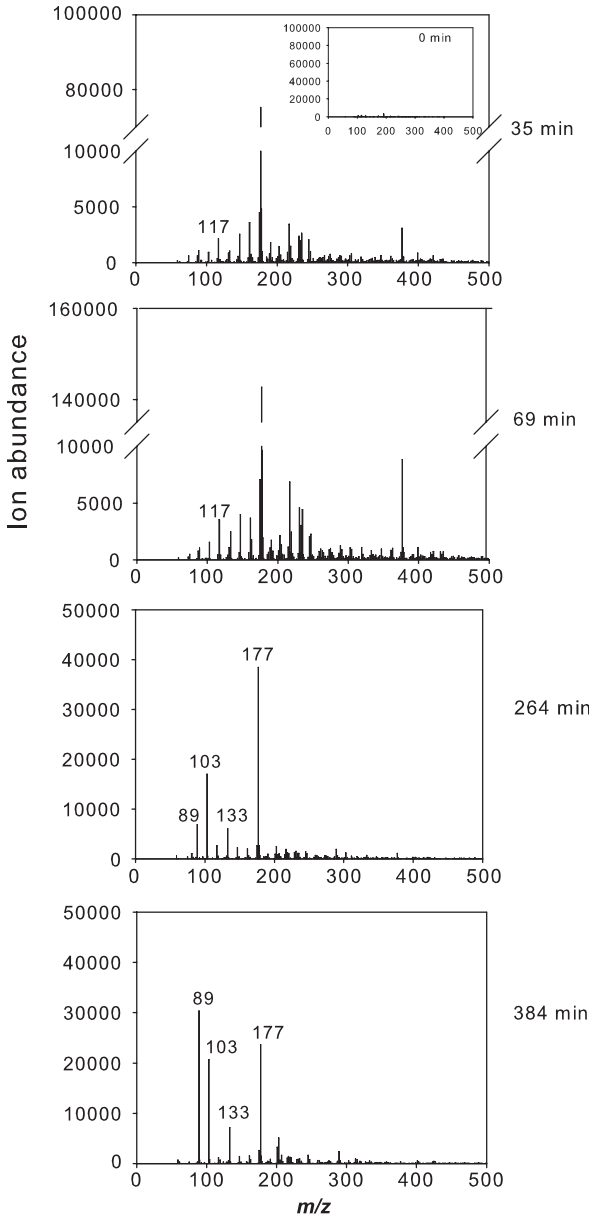

Fig. 2. ESI-MS negative ion spectra from methylglyoxal UV/H_2O_2 oxidation experimental samples. Note the different *y*-axis scale.

3.3. Oligomer properties

The 69 min experimental time series sample was chosen for negative ion FT-ICR MS analysis because at this time the oligomer formation was at a maximum in ion abundance (Fig. 2). The FT-ICR MS (9.4 T magnet) has ultra-high resolution ($m/\Delta m_{50\%} > 100{,}000$, in which $\Delta m_{50\%}$ is mass spectral peak full-width at half-maximum peak height) allowing separation of individual compounds, and mass accuracy < 1 ppm allowing exact molecular formula assignments for each compound (Marshall et al., 1998). The molecular formulas were used to calculate the organic matter to organic carbon (OM:OC) ratio of each compound in the sample, to construct a Van Krevelen diagram, and to analyze series of compounds related by regular elemental differences.

The OM:OC ratios of *m*/*z* 245–800 ranged from 1.0 to 2.5 with an average ratio (arithmetic mean) of 2.0 (Fig. 5)—comparable to the OM:OC ratio of the precursor methylglyoxal (2.0), and lower than that of the organic acid monomer products (2.3–3.8) in the proposed reaction scheme (Fig. 1, solid arrows). OM:OC is primarily driven by the oxygen content of the compound (Pang et al., 2006); therefore, we expect the oligomers to be less hygroscopic than the organic acid monomers. The ratios for the compounds in this simulated cloud water sample are consistent with bulk ratios reported in aged atmospheric aerosols (El-Zanan et al., 2005; Kiss et al., 2002) and similar to several classes of atmospherically relevant aerosol species including aliphatic dicarboxylic acids, ketocarboxylic acids, polyols (Turpin and Lim, 2001), and smog chamber generated oligomers (Kalberer et al., 2004). These similarities at the bulk level suggest that the oligomers formed in this study are similar to oligomers formed through cloud processing and aerosol phase reactions in the atmosphere.

The ultra-high resolution of FT-ICR MS allows a further level of analysis than bulk ratios because the elemental composition, and thus OM:OC, may be calculated for *each compound*. The elemental ratios were used to construct a Van Krevelen plot (Wu et al., 2004), in which the hydrogen to carbon (H:C) ratio is plotted as a function of the oxygen to carbon (O:C) ratio (Fig. 6). The average (arithmetic mean) O:C ratio was 0.69 and the average H:C ratio was 1.10 which is slightly higher than the average O:C ratios (0.4–0.6) and slightly lower than average H:C ratios (1.4–1.7) reported for particle phase oligomers formed in smog chamber experiments of α-pinene ozonolysis (Reinhardt et al., 2007). The average H:C (1.1) of the oligomers is lower than the H:C of the precursor methylglyoxal (1.3) indicating that oxidation reactions occurred.

3.4. Oligomer series

The Van Krevelen plot serves to identify a set of compounds related by regular mass differences.

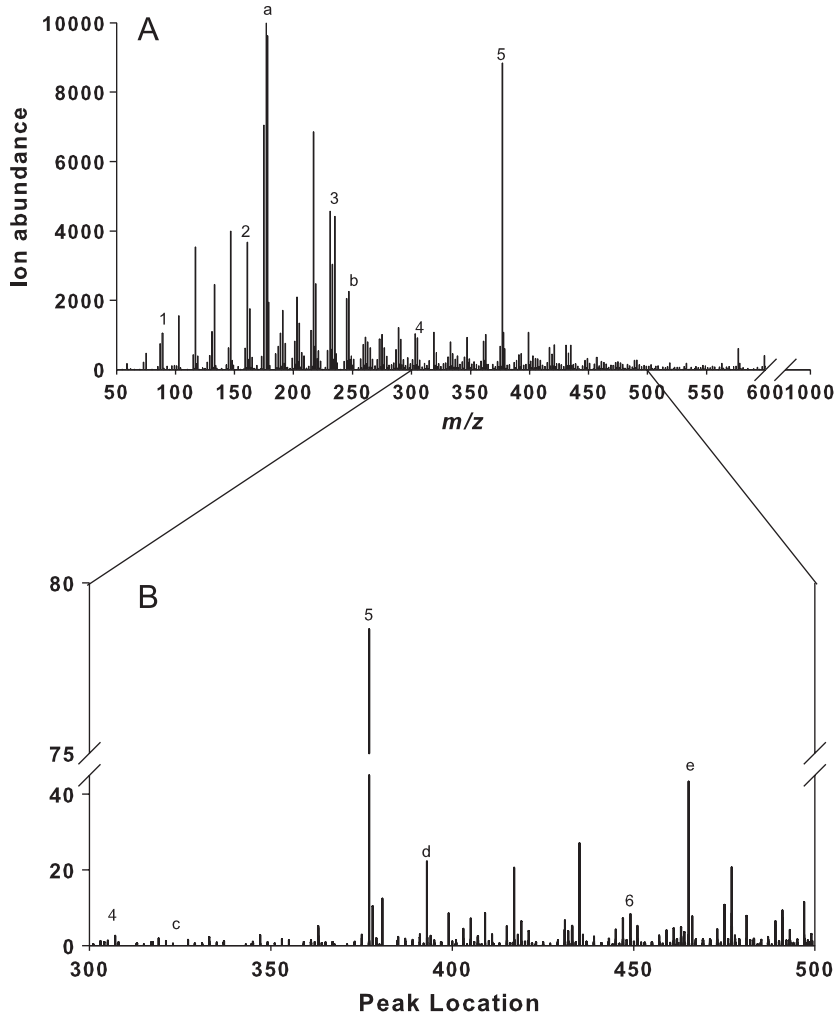

Fig. 3. The pattern of high molecular weight products from the methylglyoxal UV/H_2O_2 oxidation experiment ($t = 69$ min) analyzed by negative ion (A) ESI-MS and (B) ultra-high resolution FT-ICR MS. The ESI-MS spectrum of a mixed standard of the predicted reaction components (methylglyoxal, pyruvic acid (m/z 87), glyoxylic acid (m/z 73), oxalic acid (m/z 89) acetic acid, Fig. 4) is simple compared to the complex spectra from the photo-oxidation experimental samples. The labels 1–8 and a–e refer to the labeled compounds in Table 1. In (A) the ion abundance of m/z 177 (a), and in (B) the ion abundance of m/z 377 (5) are off scale.

There are nine series that converge on a particular point in the Van Krevelen diagram (Fig. 6, Table 1, Table S-1). This convergence point has an O:C of 0.66 and an H:C of 1.3. The difference in mass between compounds in any given series is 72.02113 which is the exact mass of a subunit ($C_3H_4O_2$) (determined by the Midas Formula Calculator Software v1.1) that repeatedly adds to the parent organic acid monomer in each of the nine series and has an O:C of 0.66 and an H:C of 1.33.

There are 65 measured compounds in the nine series. Each of the nine series (Table 1, Table S-1) consists of a parent peak (e.g., oxalic acid), and then the following m/z value represents the addition of $C_3H_4O_2$ (5–8 times) resulting in an increase in molecular weight, total oxygen content and DBE. The linear increase in DBE with each additional compound is consistent with the addition of one ring or double bond (McLafferty and Turecek, 1993; Pellegrin, 1983). Because of the consistency in detected masses between the ESI-MS and FT-ICR MS, elemental compositions assigned to compounds of $m/z > 300$ in the nine series detected were extended to ions detected by ESI-MS for ions of $m/z < 300$. The molecular formula assignments were extended for the series by subtracting $C_3H_4O_2$ and verifying the presence of ions of the corresponding m/z in the ESI-MS spectra.

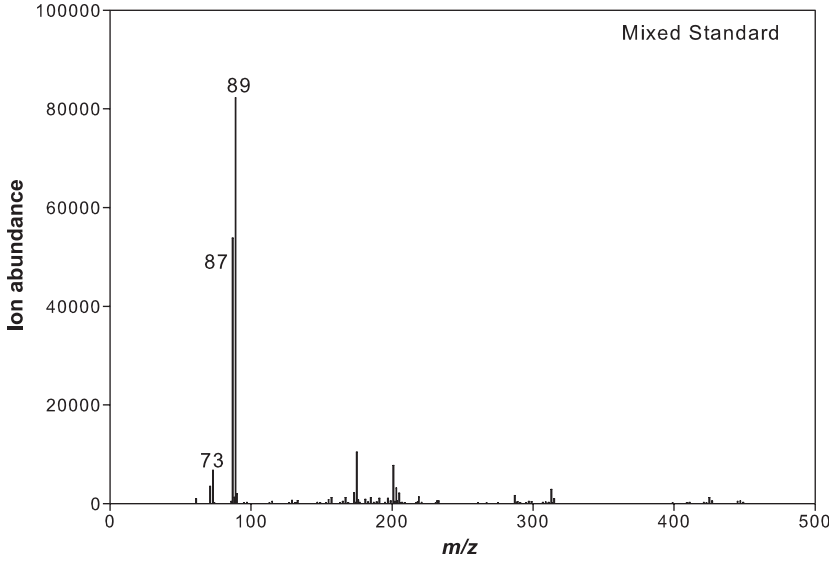

Fig. 4. ESI-MS negative ion spectra of 0.5 mM (per compound) mixed standard of methylglyoxal (detected as positive ion), oxalic acid (m/z 89), pyruvic acid (m/z 87), glyoxylic acid (m/z 73), acetic acid (not detected), in the same matrix as samples (H_2O_2 1:5 ratio, 1 μL catalase). These are the precursor and expected products in the mechanism used by (Lim et al., 2005).

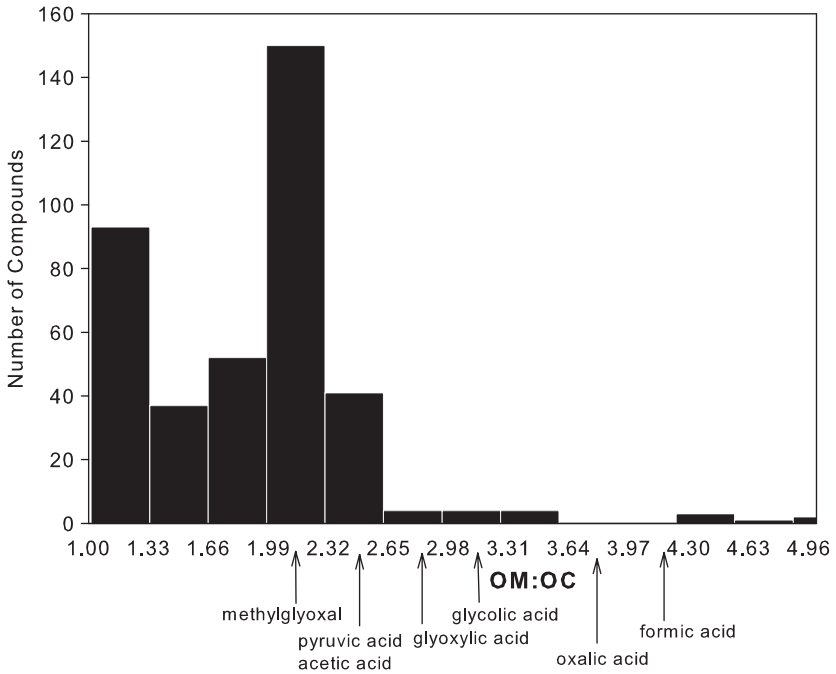

Fig. 5. Calculated OM:OC ratio (organic molecular weight per carbon weight) distribution for ions of each of the 415 m/z's from the $t = 69$ min methylglyoxal UV/H_2O_2 oxidation FT-ICR MS ($m/z > 300$ only) negative ion spectrum. The OM:OC ratios of the precursor methylglyoxal and the predicted organic acid monomers ($m/z < 300$) are noted. Each y-value is the number of compounds that had an OM:OC ratio in the bin labeled on the x-axis.

The compounds in the nine series identified (Table 1, Table S-1, Fig. 6) account for 71% of the total ion abundance in the 69 min ESI-MS negative ion sample spectrum. In seven of the series, the parent compound has been identified as an organic acid monomer (Fig. 1, Table 2). Four of the series begin with organic acids included in the reaction scheme used by Lim et al. (2005) and

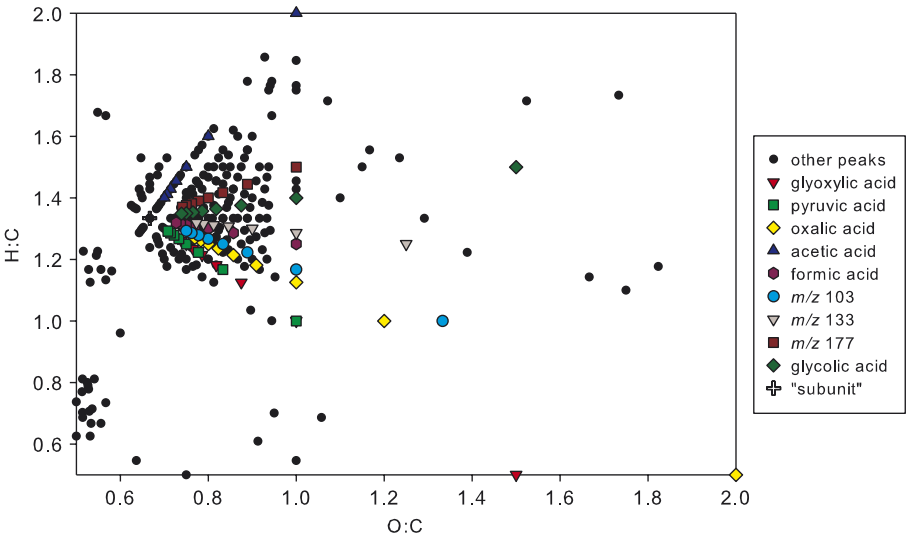

Fig. 6. Van Krevelen plot for the methylglyoxal UV/H_2O_2 oxidation experiment ($t = 69$ min) FT-ICR MS negative ion data. All of the peaks with molecular formulas assigned ($m/z > 300$) are represented by black circles. Note that only compounds with O:C and H:C > 0.5 are visible. The nine oligomer series are denoted by different symbols labeled in the legend according to the parent compound of each series. The subunit is denoted by the red "x" and is not a data point. The nine series include compounds detected by ESI-MS ($m/z < 300$) that were assigned an elemental composition based on the repeating pattern of subunit addition ($C_3H_4O_2$).

Table 1
Two examples of series of compounds starting with the parent organic acid and differing in mass by 72.02113, which is equivalent to $C_3H_4O_2$, are grouped to show the regular increase in mass, DBE, and elemental composition within the series

Label	m/z (measured)	Formula $[M-H]^-$	DBE[a]	Mass error (ppm)
1	89	$C_2H_1O_4$	2	–
2	161	$C_5H_5O_6$	3	–
3	233	$C_8H_9O_8$	4	–
4	305.05163	$C_{11}H_{13}O_{10}$	5	0.7
5	377.07274	$C_{14}H_{17}O_{12}$	6	0.5
6	449.09398	$C_{17}H_{21}O_{14}$	7	0.7
7	521.11503	$C_{20}H_{25}O_{16}$	8	0.4
8	593.13631	$C_{23}H_{29}O_{18}$	9	0.6
a	177	$C_6H_9O_6$	2	–
b	249.06175	$C_9H_{13}O_8$	3	0.6
c	321.08295	$C_{12}H_{17}O_{10}$	4	0.7
d	393.10417	$C_{15}H_{21}O_{12}$	5	0.8
e	465.12534	$C_{18}H_{25}O_{14}$	6	0.8
f	537.14629	$C_{21}H_{29}O_{16}$	7	0.3
g	609.16781	$C_{24}H_{33}O_{18}$	8	0.9

The series of formulas starting with oxalic acid (m/z 89) and m/z 177 are distinguished by the labels numeral (1–9), and letter (a–h), respectively, here and in Fig. 3. "–" indicates that the mass was detected using the ESI-MS and the elemental formula was assigned based on the "subunit" series.

[a]Double bond equivalents (number of rings plus double bonds) for neutral compound.

Table 2
Parent organic acids formed through methylglyoxal–hydroxyl radical reaction

Label	m/z (measured)	Formula $[M-H]^-$	DBE[a]
1	89	$C_2H_1O_4$	2
a	177	$C_6H_9O_6$	2
nl	73	$C_2H_1O_3$	2
nl	87	$C_3H_3O_3$	2
nl	75	$C_2H_3O_3$	1
nl	103	$C_3H_3O_4$	2
nl	117	$C_4H_5O_4$	2
nl	133	$C_4H_5O_5$	2
nl	131	$C_5H_7O_4$	2

These organic acids then undergo oligomerization reactions with a hydroxy acid forming series of oligoesters (example series in Table 1, full series in Table S-1). Oxalic acid (m/z 89) and m/z 177 are distinguished by the labels numeral (1–9) and letter (a–h), respectively, here and in Fig. 3. "nl" indicates the mass is not labeled in Fig. 3.

[a]Double bond equivalents (number of rings plus double bonds) for neutral compound.

verified by HPLC (Carlton, 2006). These are pyruvic acid (m/z 87), glyoxylic acid (m/z 73), oxalic acid (m/z 89), acetic acid (Fig. 1, solid arrows; Table 2). In the series that begins with m/z 131 ($C_5H_7O_4$), the subtraction of one subunit ($C_3H_4O_2$) leaves a

compound consistent with acetic acid as the parent compound ($C_2H_3O_2$). To verify the structure of m/z 131, the ESI-MS-MS was used to isolate and fragment the ion. The ESI-MS-MS of m/z 131 produces fragments consistent with carboxylic acid (−44, −62, −18) and a fragment (−72) consistent with the loss of one subunit ($C_3H_4O_2$, 72 Da) leaving acetic acid as the parent molecule (Fig. S-3).

Additional organic acid monomers (Fig. 1, dashed arrows) were not included in the mechanism modeled by Lim et al. (2005). One series begins with glycolic acid (m/z 75, Table 2), a proposed intermediate in the hydroxyl radical oxidation of acetic acid to oxalic acid (Stefan et al., 1996). Another series begins with succinic acid (m/z 117 in Fig. 2, Table 2), which was experimentally demonstrated to form from acetyl radical recombination in a pulse radiolysis study of acetic acid–hydroxyl radical reactions (Wang et al., 2001).

In addition to oxalic acid, there are three parent monomers (m/z 103, 133, 177, Table 2) that persist until the last time series sample (Fig. 2). We propose that the compound at m/z 133 $C_4H_6O_5$ (Table 2, Fig. 2) is malic acid (MW 134), which we suggest is formed from the reaction of succinic acid and hydroxyl radical (Fig. 7). Multiple compounds are consistent with m/z 103 (Fig. 2) and an elemental composition $C_3H_4O_4$ (Table 2) (e.g., hydroxypyruvate, malonic acid, 2-hydroxy-3-oxopropanoate). Hydroxypyruvate has been hypothesized to form through the hydroxyl radical oxidation of pyruvic acid (Stefan and Bolton, 1999), but was not experimentally verified. ESI-MS-MS was used to isolate and fragment m/z 103 in order to assign a structure. However, the fragmentation pattern of m/z 103 in the ESI-MS-MS does not allow an exact structural assignment because the main loss is −44 (CO_2) (McLafferty and Turecek, 1993) which is consistent with the carboxylic acid functionality of hydroxypyruvate, malonic acid, and 2-hydroxy-3-oxopropanoate. Two potential compounds could correspond to m/z 177, $C_6H_{10}O_6$, and $C_5H_6O_7$. The second is consistent with an oxalic acid–pyruvic acid dimer. Evidence for the formation of an oxalic acid–pyruvic acid dimer was presented previously (Altieri et al., 2006). ESI-MS-MS was used to isolate and fragment m/z 177 and the loss of fragments consistent with pyruvic and oxalic acids (−88, −90) supports the hypothesis that one of the compounds is an oxalic and pyruvic acid dimer.

3.4.1. Oligomerization mechanism

We propose acid catalyzed esterification involving the addition of a hydroxy acid $C_3H_6O_3$ to each organic acid monomer parent (Fig. 8). The hydroxy acid could be lactic acid, an α-hydroxy acid, or hydracrylic acid, a β-hydroxy acid. The addition of lactic acid to the standard mix did not cause an oligomer system to develop, which supports our previous assertion that the oligomers are not artifacts of the electrospray process. The addition of the hydroxy acid through esterification (5–8 times) results in the addition of $C_3H_4O_2$ to each parent molecule, increasing the molecular weight by 72.0213 and the DBE by one, resulting in the series of oligoesters (Table 1, Table S-1) described above. Oligomerization might be limited to the addition of 5–8 subunits in the reaction vessel because precursors are not continuously supplied. However, the average molecular weight of HULIS in atmospheric aerosols is 200–300 Da suggesting that atmospheric oligomer formation does not proceed further (Graber and Rudich, 2006).

The repeated addition of hydroxy acid through esterification is supported by the ESI-MS-MS fragmentation patterns of the oligomers in the series. The oligomers' fragmentation patterns result in losses of −72 and −88 from the first subunit fragmentation and losses of −144 and −160 consistent with the loss of the second subunit (Fig. 9). Those products are consistent with cleavage of the ester bond on both sides (McLafferty and Turecek, 1993). Structural information was obtained for 54 of the compounds in the oligomer series by isolating and fragmenting the ion by ESI-MS-MS. Of the 54 ions targeted for fragmentation, 50 had fragments consistent with the loss of one subunit (−72, −88), and 28 also had fragments consistent with the loss of the second subunit (−144, −160).

The formation of the hydroxy acid initiates esterification reactions. The difference in structure between lactic acid and hydracrylic acid is the positioning of the hydroxy group on the carbon α or β to the carboxylic acid functionality. We do not have a proposed pathway for lactic acid formation in these experiments. However, we do propose a mechanism in which the formation of hydracrylic acid, the β-hydroxy acid, is possible from the reaction of succinic acid with hydroxyl radical (Fig. 7). The proposed mechanism is analogous to the reactions of carboxylic acids and hydroxyl radicals described by Stefan and Bolton (1999)

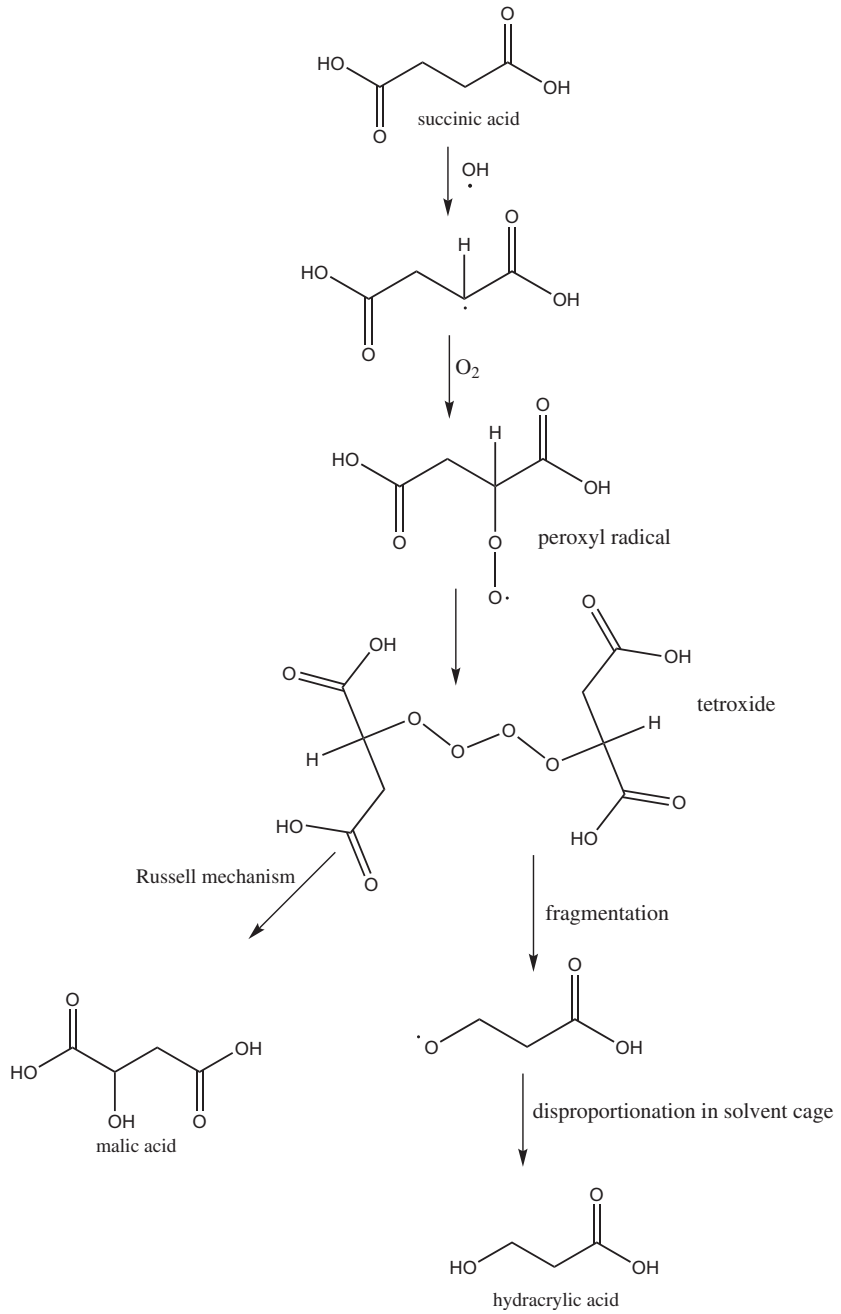

Fig. 7. Proposed mechanism of hydracrylic acid and malic acid formation from succinic acid.

and Stefan et al. (1996). Briefly, the degradation of succinic acid proceeds by a hydrogen abstraction and subsequent peroxyl radical formation through the addition of molecular oxygen (Alfassi, 1997). The second step involves the formation of a tetroxide which can undergo multiple degradation reactions including disproportionation to malic acid and fragmentation to a radical species (Stefan et al., 1996). The radical undergoes disproportionation in the solvent cage to yield hydracrylic acid (Stefan and Bolton, 1999; Stefan et al., 1996 and references therein).

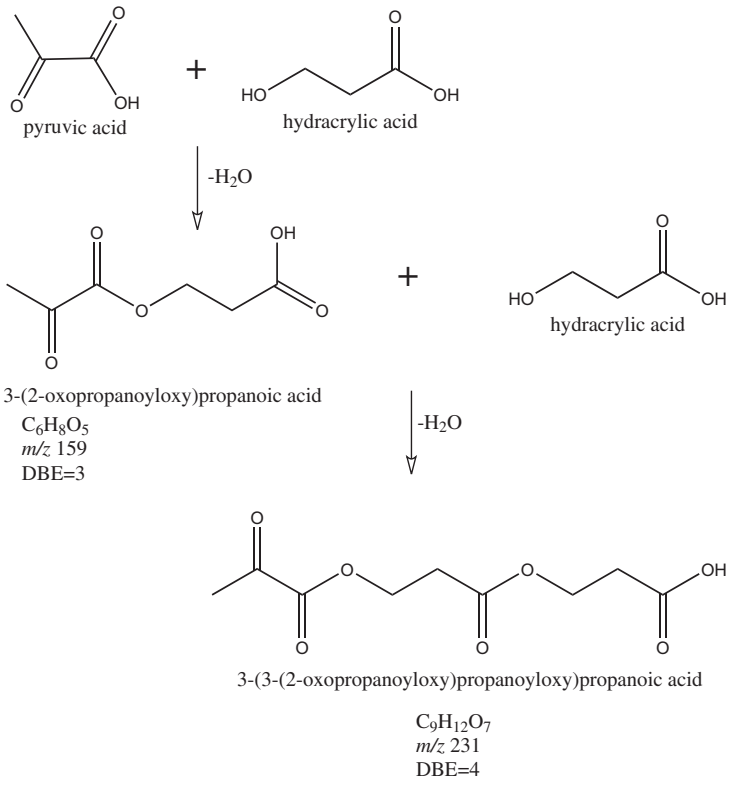

Fig. 8. Proposed non-radical esterification reactions that lead to oligomeric products. The loss of water at each step causes the higher molecular weight oligomers to have a lower OM:OC than the parent organic acid monomers. The repeating addition of hydracrylic acid creates the constant increase of $C_3H_4O_2$ in the series (Table 1, Table S-1). The oligomer species are named by use of the ChemDraw Ultra 10.0 "structure to name" algorithm.

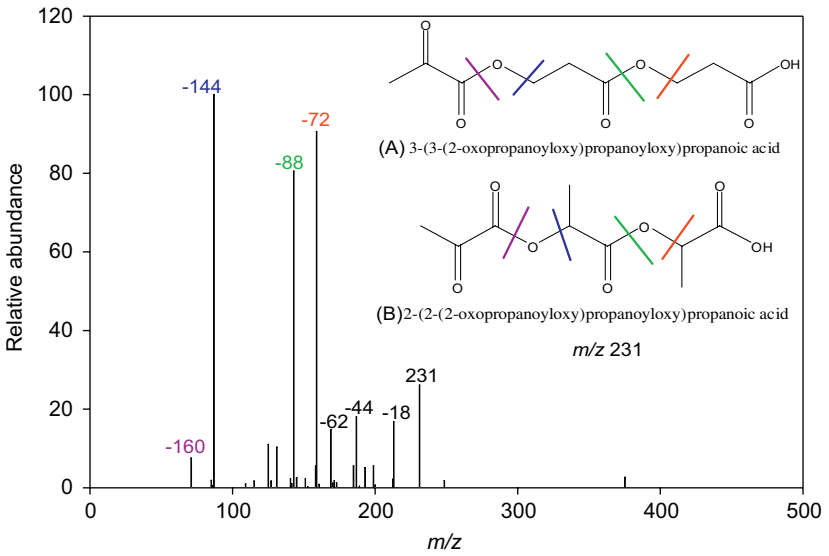

Fig. 9. ESI-MS-MS (negative ion) of m/z 231 from $t = 129$ min methylglyoxal–hydroxyl radical photo-oxidation experiments. The two hypothesized structures in the upper right hand corner are based on the esterification mechanism with (A) hydracrylic acid and (B) lactic acid, and the elemental composition assignments from the oligomer series (parent is pyruvic acid, Table 2). The colored lines on the structure indicate the bond that fragments to give ions of the m/z labeled (corresponding color) with the weight of the fragment lost.

4. Conclusions and implications

The formation of oxalic acid and higher molecular weight oligomer products from methylglyoxal photo-oxidation has been confirmed. This work adds to the growing body of literature (Altieri et al., 2006; Carlton et al., 2006, 2007; Crahan et al., 2004; Warneck, 2003; Yu et al., 2005) supporting the hypothesis that cloud processing is a significant source of oxalic acid, the most abundant dicarboxylic acid in the atmosphere. Organic acids (especially oxalic, pyruvic, and succinic acids (Saxena and Hildemann, 1996)) and the low volatility oligomer products will contribute to SOA upon cloud droplet evaporation. The varied and multiple sources of methylglyoxal increase the potential for this pathway to contribute significantly to SOA through cloud processing. The OM:OC ratios of the oligomers are comparable to aged atmospheric aerosols, and lower than those of prevalent organic acids suggesting that the oligomers are less hygroscopic than the organic acids and consistent with the growing belief that oligomers are a large contributor to aged organic aerosol mass.

Organic acid monomers form from aqueous reactions with hydroxyl radical. The oligomerization of these organic acid monomers then proceeds through esterification with an α- or β-hydroxy acid. This mechanism is supported by the high-resolution elemental composition data and the ESI-MS-MS fragmentation data. The esterification causes the regular addition of $C_3H_4O_2$ to the organic acid monomers resulting in series of oligoesters related by regular differences in elemental composition and mass. The esterification mechanism proposed in this work is similar to mechanisms proposed for oligomers formed in the aerosol phase (Gao et al., 2004; Surratt et al., 2006, 2007), which have been reported to be thermodynamically favorable (Barsanti and Pankow, 2006). In both aerosol phase and cloud processing reactions (aqueous phase), the oligomers formed are less hygroscopic and less volatile than the low molecular weight compounds that lead to their formation. Multiple precursor organics lead to oligomer products through similar mechanisms in both aerosol phase reactions (e.g., isoprene, α-pinene, trimethylbenzene) and cloud processing reactions (e.g., methylglyoxal, pyruvic acid). The similarities in properties and formation mechanisms of oligomers may help to explain the large quantity of oligomers found in atmospheric particles.

Acknowledgments

This research has been supported by a grant from the US Environmental Protection Agency's Science to Achieve Results (STAR) Program (R831073), and the USA National Science Foundation (ATM-0630298 and DMR-00-84173). This research was also performed, in part, under the Memorandum of Understanding between the US Environmental Protection Agency (EPA) and the US Department of Commerce's National Oceanic and Atmospheric Administration (NOAA) and under agreement number DW13921548. This work constitutes a contribution to the NOAA Air Quality Program. Although it has been reviewed by EPA and NOAA and approved for publication, it does not necessarily reflect their policies or views. We thank Ho-Jin Lim for his modeling study that inspired this work. We also gratefully acknowledge useful conversations with Dr. Jeehuin Lee, Dr. Mark Perri, and Yi-Tan.

Appendix A. Supplementary materials

Supplementary data associated with this article can be found in the online version at doi:10.1016/j.atmosenv.2007.11.015.

References

Alfassi, Z.B. (Ed.), 1997. Peroxyl Radicals. Wiley, Chichester, UK.

Altieri, K.E., Carlton, A.G., Lim, H.J., Turpin, B.J., Seitzinger, S.P., 2006. Evidence for oligomer formation in clouds: reactions of isoprene oxidation products. Environmental Science and Technology 40 (16), 4956–4960.

Atkinson, R., 2000. Atmospheric chemistry of VOCs and NOx. Atmospheric Environment 34 (12–14), 2063–2101.

Atkinson, R., Arey, J., 2003. Gas-phase tropospheric chemistry of biogenic volatile organic compounds: a review. Atmospheric Environment 37 (Suppl. 2), 197–219.

Barsanti, K.C., Pankow, J.F., 2006. Thermodynamics of the formation of atmospheric organic particulate matter by accretion reactions—Part 3: Carboxylic and dicarboxylic acids. Atmospheric Environment 40 (34), 6676–6686.

Blando, J.D., Turpin, B.J., 2000. Secondary organic aerosol formation in cloud and fog droplets: a literature evaluation of plausibility. Atmospheric Environment 34 (10), 1623–1632.

Carlton, A.G., 2006. Secondary Organic Aerosol (SOA) Formation through Cloud Processing: Aqueous Photooxidation of Glyoxal and Methylglyoxal. Rutgers, The State University of New Jersey, New Brunswick, USA, 237pp.

Carlton, A.G., Turpin, B.J., Lim, H.J., Altieri, K.E., Seitzinger, S., 2006. Link between isoprene and secondary organic

aerosol (SOA): pyruvic acid oxidation yields low volatility organic acids in clouds. Geophysical Research Letters 33 (6), L06822.

Carlton, A.G., Turpin, B.J., Altieri, K.E., Seitzinger, S., Reff, A., Lim, H.-J., Ervens, B., 2007. Atmospheric oxalic acid and SOA production from glyoxal: results of aqueous photooxidation experiments. Atmospheric Environment 41 (35), 7588–7602.

Crahan, K.K., Hegg, D., Covert, D.S., Jonsson, H., 2004. An exploration of aqueous oxalic acid production in the coastal marine atmosphere. Atmospheric Environment 38 (23), 3757–3764.

Denkenberger, K.A., Moffet, R.C., Holecek, J.C., Rebotier, T.P., Prather, K.A., 2007. Real-time, single-particle measurements of oligomers in aged ambient aerosol particles. Environmental Science and Technology 41 (15), 5439–5446.

El-Zanan, H.S., Lowenthal, D.H., Zielinska, B., Chow, J.C., Kumar, N., 2005. Determination of the organic aerosol mass to organic carbon ratio in IMPROVE samples. Chemosphere 60 (4), 485–496.

EPA, 2004. Air Quality Criteria for Particulate Matter. US Government Printing Office, Washington, DC.

Ervens, B., George, C., Williams, J.E., Buxton, G.V., Salmon, G.A., Bydder, M., Wilkinson, F., Dentener, F., Mirabel, P., Wolke, R., Herrmann, H., 2003. CAPRAM 2.4 (MODAC mechanism): an extended and condensed tropospheric aqueous phase mechanism and its application. Journal of Geophysical Research—Atmospheres 108 (D14), 4426.

Ervens, B., Feingold, G., Frost, G.J., Kreidenweis, S.M., 2004. A modeling study of aqueous production of dicarboxylic acids: chemical pathways and speciated organic mass production. Journal of Geophysical Research—Atmospheres 109, D15205.

Gao, S., Keywood, M., Ng, N.L., Surratt, J., Varutbangkul, V., Bahreini, R., Flagan, R.C., Seinfeld, J.H., 2004. Low-molecular-weight and oligomeric components in secondary organic aerosol from the ozonolysis of cycloalkenes and alpha-pinene. Journal of Physical Chemistry A 108 (46), 10147–10164.

Gelencser, A., Varga, Z., 2005. Evaluation of the atmospheric significance of multiphase reactions in atmospheric secondary organic aerosol formation. Atmospheric Chemistry and Physics 5, 2823–2831.

Graber, E.R., Rudich, Y., 2006. Atmospheric HULIS: how humic-like are they? A comprehensive and critical review. Atmospheric Chemistry and Physics 6, 729–753.

Guzman, M.I., Colussi, A.I., Hoffmann, M.R., 2006. Photoinduced oligomerization of aqueous pyruvic acid. Journal of Physical Chemistry A 110 (10), 3619–3626.

Ham, J.E., Proper, S.P., Wells, J.R., 2006. Gas-phase chemistry of citronellol with ozone and OH radical: rate constants and products. Atmospheric Environment 40 (4), 726–735.

Hastings, W.P., Koehler, C.A., Bailey, E.L., DeHaan, D.O., 2005. Secondary organic aerosol formation by glyoxal hydration and oligomer formation: humidity effects and equilibrium shifts during analysis. Environmental Science and Technology 39 (22), 8728–8735.

Heald, C.L., Jacob, D.J., Turquety, S., Hudman, R.C., Weber, R.J., Sullivan, A.P., Peltier, R.E., Atlas, E.L., de Gouw, J.A., Warneke, C., Holloway, J.S., Neuman, J.A., Flocke, F.M., Seinfeld, J.H., 2006. Concentrations and sources of organic carbon aerosols in the free troposphere over North America. Journal of Geophysical Research—Atmospheres 111 (D23), D23S47.

Henze, D.K., Seinfeld, J.H., 2006. Global secondary organic aerosol from isoprene oxidation. Geophysical Research Letters 33 (9), L09812.

Holmes, B.J., Petrucci, G.A., 2006. Water-soluble oligomer formation from acid-catalyzed reactions of levoglucosan in proxies of atmospheric aqueous aerosols. Environmental Science and Technology 40 (16), 4983–4989.

IPCC, 2001. Climate Change: The Scientific Basis. Cambridge University Press, UK.

Jang, M., Czoschke, N.M., Lee, S., Kamens, R.M., 2002. Heterogeneous atmospheric aerosol production by acid-catalyzed particle-phase reactions. Science 298 (5594), 814–817.

Kalberer, M., Paulsen, D., Sax, M., Steinbacher, M., Dommen, J., Prevot, A.S.H., Fisseha, R., Weingartner, E., Frankevich, V., Zenobi, R., Baltensperger, U., 2004. Identification of polymers as major components of atmospheric organic aerosols. Science 303 (5664), 1659–1662.

Kawamura, K., Yasui, O., 2005. Diurnal changes in the distribution of dicarboxylic acids, ketocarboxylic acids and dicarbonyls in the urban Tokyo atmosphere. Atmospheric Environment 39 (10), 1945–1960.

Kawamura, K., Kasukabe, H., Barrie, L.A., 1996. Source and reaction pathways of dicarboxylic acids, ketoacids and dicarbonyls in arctic aerosols: one year of observations. Atmospheric Environment 30 (10–11), 1709–1722.

Kiss, G., Varga, B., Galambos, I., Ganszky, I., 2002. Characterization of water-soluble organic matter isolated from atmospheric fine aerosol. Journal of Geophysical Research—Atmospheres 107 (D21), 8339.

Kroll, J.H., Ng, N.L., Murphy, S.M., Flagan, R.C., Seinfeld, J.H., 2006. Secondary organic aerosol formation from isoprene photooxidation. Environmental Science and Technology 40 (6), 1869–1877.

Lim, H.J., Carlton, A.G., Turpin, B.J., 2005. Isoprene forms secondary organic aerosol through cloud processing: model simulations. Environmental Science and Technology 39 (12), 4441–4446.

Loeffler, K.W., Koehler, C.A., Paul, N.M., De Haan, D.O., 2006. Oligomer formation in evaporating aqueous glyoxal and methyl glyoxal solutions. Environmental Science and Technology 40 (20), 6318–6323.

Marshall, A.G., Guan, S.H., 1996. Advantages of high magnetic field for Fourier transform ion cyclotron resonance mass spectrometry. Rapid Communications in Mass Spectrometry 10 (14), 1819–1823.

Marshall, A.G., Hendrickson, C.L., Jackson, G.S., 1998. Fourier transform ion cyclotron resonance mass spectrometry: a primer. Mass Spectrometry Reviews 17 (1), 1–35.

Martinelango, P.K., Dasgupta, P.K., Al-Horr, R.S., 2007. Atmospheric production of oxalic acid/oxalate and nitric acid/nitrate in the Tampa Bay airshed: parallel pathways. Atmospheric Environment 41 (20), 4258–4269.

Matsumoto, K., Kawai, S., Igawa, M., 2005. Dominant factors controlling concentrations of aldehydes in rain, fog, dew water, and in the gas phase. Atmospheric Environment 39 (38), 7321–7329.

McLafferty, F.W., Turecek, F., 1993. Interpretation of Mass Spectra, fourth ed. University Science Books, Mill Valley, USA.

Munger, J.W., Jacob, D.J., Daube, B.C., Horowitz, L.W., Keene, W.C., Heikes, B.G., 1995. Formaldehyde, glyoxal, and methylglyoxal in air and cloudwater at a rural mountain site in central Virginia. Journal of Geophysical Research—Atmospheres 100 (D5), 9325–9333.

Pang, Y., Turpin, B.J., Gundel, L.A., 2006. On the importance of organic oxygen for understanding organic aerosol particles. Aerosol Science and Technology 40 (2), 128–133.

Pellegrin, V., 1983. Molecular formulas of organic compounds: the nitrogen rule and degree of unsaturation. Journal of Chemical Education 60 (8), 626–633.

Reemtsma, T., These, A., Venkatachari, P., Xia, X.Y., Hopke, P.K., Springer, A., Linscheid, M., 2006. Identification of fulvic acids and sulfated and nitrated analogues in atmospheric aerosol by electrospray ionization Fourier transform ion cyclotron resonance mass spectrometry. Analytical Chemistry 78 (24), 8299–8304.

Reinhardt, A., Emmenegger, C., Gerrits, B., Panse, C., Dommen, J., Baltensperger, U., Zenobi, R., Kalberer, M., 2007. Ultrahigh mass resolution and accurate mass measurements as a tool to characterize oligomers in secondary organic aerosols. Analytical Chemistry 79 (11), 4074–4082.

Saxena, P., Hildemann, L.M., 1996. Water-soluble organics in atmospheric particles: a critical review of the literature and application of thermodynamics to identify candidate compounds. Journal of Atmospheric Chemistry 24 (1), 57–109.

Seinfeld, J.H., Pankow, J.F., 2003. Organic atmospheric particulate material. Annual Review of Physical Chemistry 54, 121–140.

Senko, M.W., Hendrickson, C.L., PasaTolic, L., Marto, J.A., White, F.M., Guan, S.H., Marshall, A.G., 1996. Electrospray ionization Fourier transform ion cyclotron resonance at 9.4 T. Rapid Communications in Mass Spectrometry 10 (14), 1824–1828.

Senko, M.W., Hendrickson, C.L., Emmett, M.R., Shi, S.D.H., Marshall, A.G., 1997. External accumulation of ions for enhanced electrospray ionization Fourier transform ion cyclotron resonance mass spectrometry. Journal of the American Society for Mass Spectrometry 8 (9), 970–976.

Smith, D.F., Kleindienst, T.E., McIver, C.D., 1999. Primary product distributions from the reaction of OH with *m*-, *p*-xylene, 1,2,4- and 1,3,5-trimethylbenzene. Journal of Atmospheric Chemistry 34 (3), 339–364.

Sorooshian, A., Ng, L., Chan, A.W.H., Feingold, G., Flagan, R.C., Seinfeld, J.H., 2007. Particulate organic acids and overall water-soluble aerosol composition measurements from the 2006 Gulf of Mexico Atmospheric Composition and Climate Study (GoMACCS). Journal of Geophysical Research—Atmospheres 112.

Stefan, M.I., Bolton, J.R., 1999. Reinvestigation of the acetone degradation mechanism in dilute aqueous solution by the UV/H_2O_2 process. Environmental Science and Technology 33, 870–873.

Stefan, M.I., Hoy, A.R., Bolton, J.R., 1996. Kinetics and mechanism of the degradation and mineralization of acetone in dilute aqueous solution sensitized by the UV photolysis of hydrogen peroxide. Environmental Science and Technology 30, 2382–2390.

Surratt, J.D., Murphy, S.M., Kroll, J.H., Ng, N.L., Hildebrandt, L., Sorooshian, A., Szmigielski, R., Vermeylen, R., Maenhaut, W., Claeys, M., Flagan, R.C., Seinfeld, J.H., 2006. Chemical composition of secondary organic aerosol formed from the photooxidation of isoprene. Journal of Physical Chemistry A 110 (31), 9665–9690.

Surratt, J.D., Kroll, J.H., Kleindienst, T.E., Edney, E.O., Claeys, M., Sorooshian, A., Ng, N.L., Offenberg, J.H., Lewandowski, M., Jaoui, M., Flagan, R.C., Seinfeld, J.H., 2007. Evidence for organosulfates in secondary organic aerosol. Environmental Science and Technology 41 (2), 517–527.

Tolocka, M.P., Myoseon, J., Joy, M.G., Frederick, J.C., Richard, M.K., Murray, V.J., 2004. Formation of oligomers in secondary organic aerosol. Environmental Science and Technology 38 (5), 1428–1434.

Turpin, B.J., Lim, H.J., 2001. Species contributions to PM2.5 mass concentrations: revisiting common assumptions for estimating organic mass. Aerosol Science and Technology 35 (1), 602–610.

Wang, W.F., Schuchmann, M.N., Schuchmann, H.P., von Sonntag, C., 2001. The importance of mesomerism in the termination of alpha-carboxymethyl radicals from aqueous malonic and acetic acids. Chemistry—A European Journal 7 (4), 791–795.

Warneck, P., 2003. In-cloud chemistry opens pathway to the formation of oxalic acid in the marine atmosphere. Atmospheric Environment 37 (17), 2423–2427.

Wilcox, B.E., Hendrickson, C.L., Marshall, A.G., 2002. Improved ion extraction from a linear octopole ion trap: SIMION analysis and experimental demonstration. Journal of the American Society for Mass Spectrometry 13 (11), 1304–1312.

Wu, Z.G., Rodgers, R.P., Marshall, A.G., 2004. Two- and three-dimensional van Krevelen diagrams: a graphical analysis complementary to the Kendrick mass plot for sorting elemental compositions of complex organic mixtures based on ultrahigh-resolution broadband Fourier transform ion cyclotron resonance mass measurements. Analytical Chemistry 76 (9), 2511–2516.

Yu, J.Z., Huang, X.F., Xu, J.H., Hu, M., 2005. When aerosol sulfate goes up, so does oxalate: implication for the formation mechanisms of oxalate. Environmental Science and Technology 39 (1), 128–133.